Assimilation of data into an ocean model with systematic errors near the equator

Ocean Applications Technical Note No. 27

M.J. Bell, M.J. Martin and N.K. Nichols

March 2001

Summary

Assimilation of thermal data into an ocean model near the equator often results in a dynamically unbalanced state with unrealistic deep overturning circulations. The way in which these circulations arise from errors in the model or its forcing and the equatorial dynamics is discussed. A scheme is proposed to calculate a state with a better balance by using the observational increments to the model to update slowly evolving bias fields. These bias fields augment the model state and affect the model's pressure gradients. The properties of the augmented shallow water equations are examined. When forced by steady incorrect wind stresses, solutions of the augmented equations assimilating full fields of surface height data converge to the correct surface height and vertical velocity fields. Results from an experiment applying this bias correction scheme to an ocean general circulation model are summarised. They show that the method produces more balanced analyses and a better fit to temperature observations.

1. Introduction

Assimilation of data into ocean models is becoming increasingly viable. Substantial in situ real-time observing networks such as the TAO buoy array (Busalacchi 1995) and the ARGO (1999) array of autonomous profiling floats have been or are being deployed. Satellite measurements of the surface wind stress and sea surface height are also available for assimilation by operational centres.

A particular problem for seasonal forecasting is that, unless particular care is taken, ocean models do not retain the observational data assimilated into them for more than a few months but drift away towards their own climatologies in the key regions of variability within a few degrees of the equator. Ji & Leetma (1997) address this problem by careful choice of the time-mean wind stress used to force their models and by calculating observed anomalies and assimilating them as anomalies from their model's climatology. Alternative approaches using variational schemes include the works of Yu & O'Brien (1991), who trialled a variational assimilation scheme in which the wind stress field is a control variable, and Derber (1992), who developed a continuous variational assimilation formulation specifically to address the problem of model bias. In the latter scheme the control variable is the field of heating/cooling required to prevent the model from drifting. Of particular relevance to this paper are some studies in the context of Kalman filters. Friedland (1969) proposed augmenting the state vector by a model bias vector and transforming the gain matrices of the Kalman filter to produce a computationally cheaper

method. Dee & Da Silva (1998), hereafter referred to as DDS, have applied this idea to numerical weather prediction (NWP).

In this paper we build on the ideas of DDS by developing a formulation of the augmented state method to produce balanced analyses near the equator. Section 2 illustrates the spurious vertical circulations and time-mean observational temperature increments made when temperature observations are assimilated into an ocean general circulation model (OGCM) near the equator. Section 3 discusses the dynamics of these circulations and a method for suppressing them is described in section 4. Section 4.1 briefly reviews the theory of augmenting the state and 4.2 describes what we term the "pressure correction" method which combines the ideas from sections 3 and 4.1. This method involves augmenting the model state by a bias error variable and incrementing this bias using the observational increments in a specific way. The characteristics of the method, when it is applied to the shallow water equations forced by incorrect wind stresses, are explored in section 5. Particular attention is given to the conditions under which the solution will converge to the truth and the rate of convergence. Section 6 compares our method with the assimilation of anomalies from climatology and DDS's methods. It also discusses the application of the method to seasonal forecasting and some directions for future research. Section 7 is a concluding summary.

This report will form the basis of Part I of a paper. Part II will present some results from the application of the pressure correction method to two OGCMs. Some preliminary results from the application of the pressure corrrection method to the Met Office OGCM system are shown in Appendix B.

2. Problems arising from data assimilation near the equator

The problems which arise are illustrated in this section using two integrations described in detail in Bell et al. (2000). The first assimilates surface temperature and thermal profile data. The second is identical to the first except that no data is assimilated. The integrations start from a state of rest with potential temperatures and salinities derived from the Levitus (1994) climatology for the 1st May. They are forced by monthly mean climatological fluxes. The wind stresses are taken from Hellerman & Rosenstein (1983) which are generally regarded as being too strong in the equatorial regions. The model has global coverage, uses a latitude-longitude grid with 1° resolution and has 20 levels in the vertical. It is based on the Cox (1984) code and includes parametrisations of vertical mixing developed for coupled climate modelling. The data assimilation component is based on the analysis correction scheme of Lorenc et al. (1991). The estimated error variance for each observation is set equal to that assigned to the model field. The horizontal error correlation scale used is 300 km, except within a few degrees of the equator. At the equator the scale is 600 km along the equator and 150 km across it. Each thermal profile observation is assimilated over a period of 20 days centred on its time of validity. No salinity data are used and no salinity increments are made by the assimilation scheme. Observations valid from the 1st May 1995 to 30th April 1996 were assimilated. Neither an El Nino nor a La Nina event occurred during this period. The integrations presented ran for two years. The data assimilation run assimilated the same data in both years of integration.

Figures 1(a) and 1(b) show the time mean of the potential temperature field along the equator in the Pacific for the second year of the control and assimilation integrations respectively. It is clear from these plots that the assimilation acts to tighten the thermocline so that the temperature

gradient is much steeper with data assimilation. Although the systematic bias in our control integration may be slightly larger than in some other systems, because of the use of the Hellerman wind stresses and a model with relatively poor north-south resolution near the equator, it is difficult to eliminate biases of this nature from coupled ocean-atmosphere models (Stockdale et al. 1993, Fevrier et al. 2000).

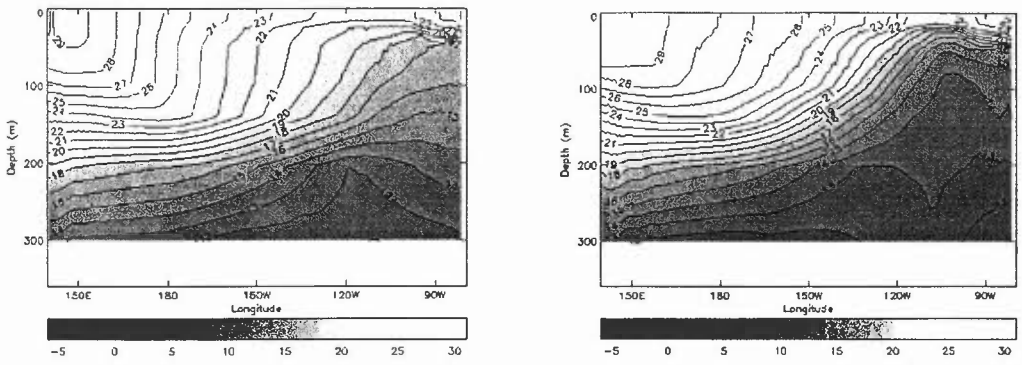

Figure 1. Annual mean (2nd Year) potential temperature (°C) cross-section along equator between 140°E – 90°W: (a) control without data assimilation and (b) with data assimilation.

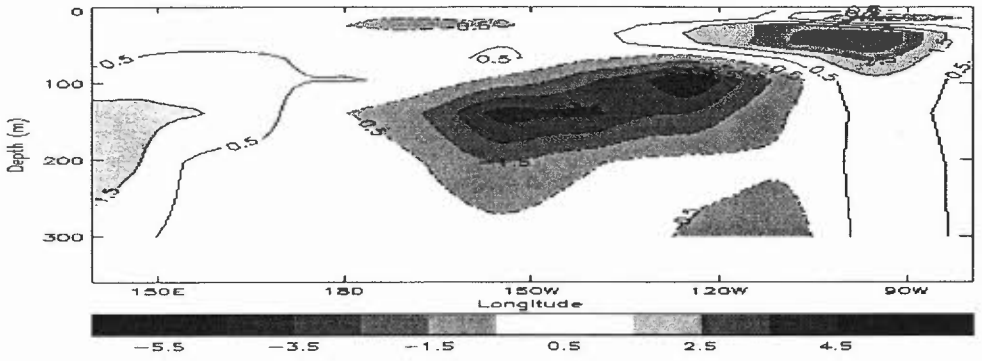

Figure 2. Annual mean (2nd Year) potential temperature increments (°C month^{-1}) cross-section along equator between 140°E-90°W for run with data assimilation.

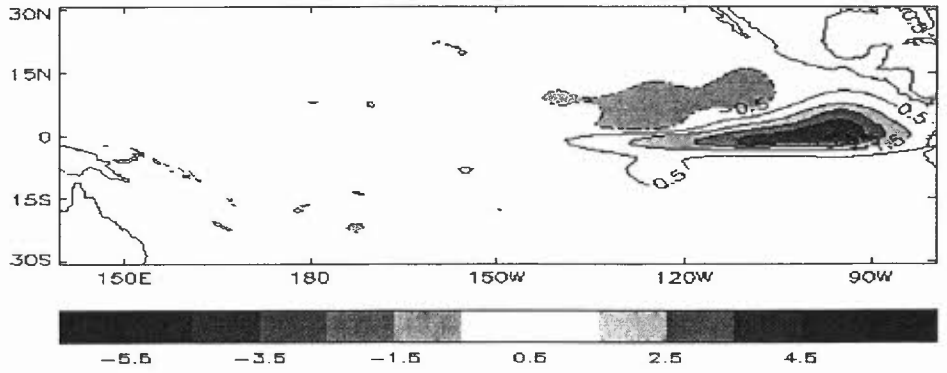

Figure 3. Annual mean (2nd Year) potential temperature increments (°C month^{-1}) field at about 50m depth for the run with data assimilation.

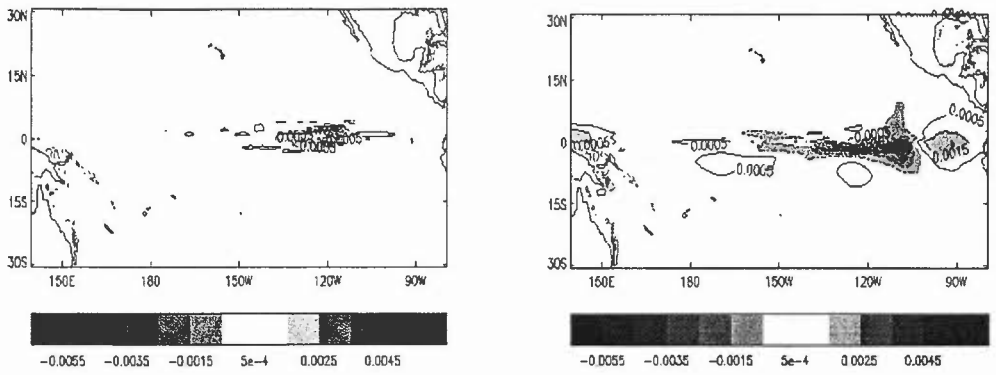

Figure 4. Annual mean (2nd Year) vertical velocities (cm s^{-1}) field at about 250m depth: (a) control without data assimilation and (b) with data assimilation.

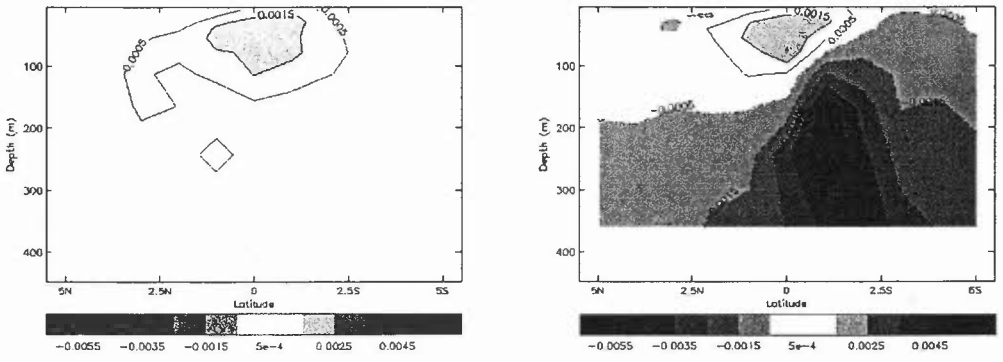

Figure 5. Annual mean (2nd Year) vertical velocities (cm s^{-1}) cross-section across equator at 110°W: (a) control without data assimilation and (b) with data assimilation.

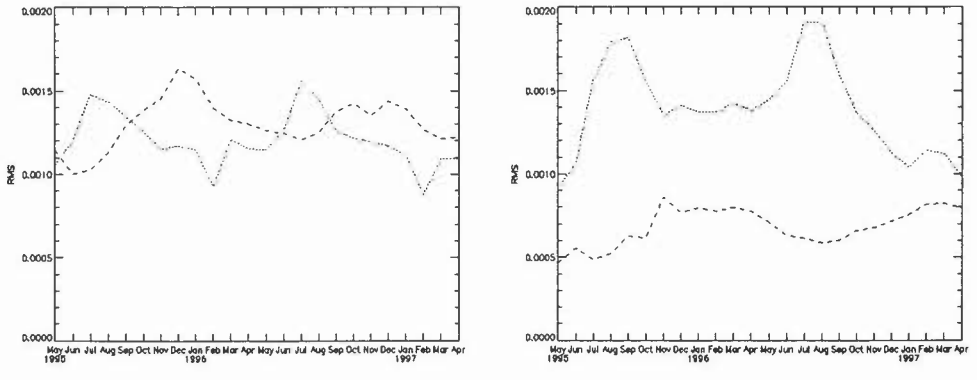

Figure 6. Root mean square values of monthly mean vertical velocities over the region 5°N-5°S, 140°E-80°W: (a) at about 50m depth and (b) at about 250m depth. Dashed – control without data assimilation. Dotted – with data assimilation.

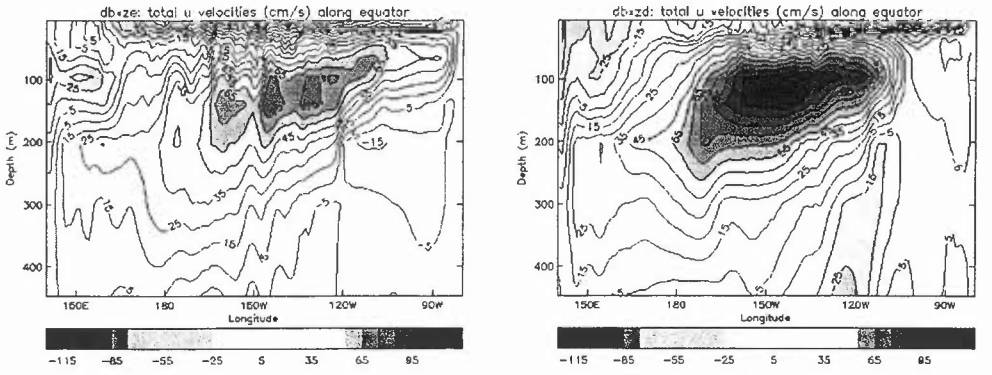

Figure 7. Annual mean (2nd Year) zonal velocity (cm s^{-1}) along the equator between 140°E-90°W: (a) control without data assimilation and (b) with data assimilation.

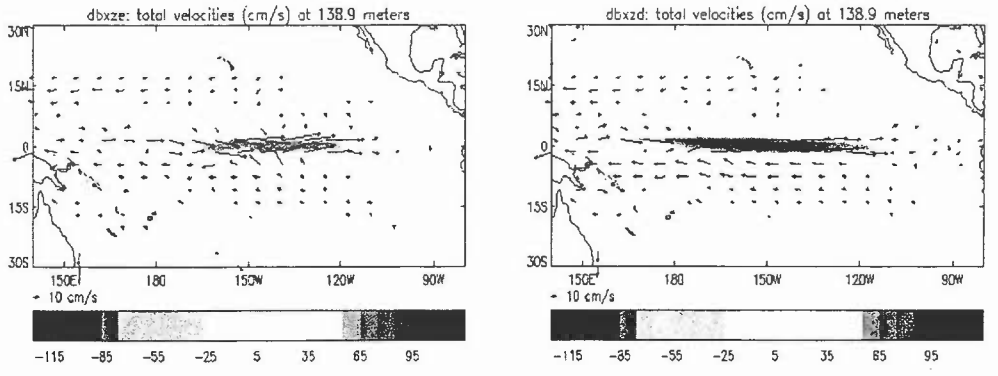

Figure 8. Annual mean (2nd Year) total velocity (cm s^{-1}) field at about 140m depth: (a) control without data assimilation and (b) with data assimilation.

Figure 2 shows the time-mean cross-section of the potential temperature increments made by the data assimilation component during the second year of the assimilation along the same section as Fig. 1. The increments are very large, exceeding 1.5°C $month^{-1}$ over large areas. This indicates that in these regions over the course of the second year of integration the data assimilation warmed/cooled the ocean by more than 18°C and the ocean model cooled/warmed the ocean by similar amounts. Thus the ocean model cannot be considered to be in a satisfactory dynamical balance during the assimilation, and any forecast made from an assimilation state is likely to drift very rapidly during the first months of the forecast. Figure 3 shows a horizontal view of the time-mean potential temperature increments at about 50m depth. The increments are confined to within 15 degrees of the equator with the strongest increments being applied very close to the equator. There are also large time mean temperature increments in the areas of the Gulf Stream and Kurushio currents not shown here but we do not attempt to examine these regions.

The time mean fields of vertical velocities near 250m depth for the control and assimilation runs are displayed in Figs. 4(a) and (b) respectively. It appears from these plots that the data assimilation is inducing unrealistically large time-mean vertical velocities at this depth. The vertical cross-sections of the vertical velocity at 110°W shown in Figs. 5(a) and (b) support this conjecture. Figures 6(a) and (b) show the root mean square (rms) values of the monthly mean

vertical velocities over the region 5°N-5°S, 140°E-80°W as timeseries for the second year of integration at two depths for the control and assimilation runs. They show that at 50m depth the vertical velocities in the two runs are similar in magnitude but that at 250m depth the magnitude of the vertical velocities is much stronger in the run with data assimilation included.

Figures 7(a) and (b) show the zonal velocity along the equator for the same sections and integrations as Figs. 1 and 2. The wind-driven near surface westward current and the eastward equatorial undercurrent are clearly apparent in the control integration, though the maximum strength of the undercurrent at 80 cm s^{-1} is slightly weaker than it is observed to be (120 cm s^{-1}). In the assimilation experiment, the undercurrent does not penetrate as far to the east in the model as it should do and the surface currents are reversed at about 150°W. Westward flowing currents to the north and south of the equator at about 150m depth can be seen for both the control run and the run with data assimilation in Figs. 8(a) and (b) respectively. The run with data assimilation has much stronger horizontal velocities both in the equatorial undercurrent and in the current to the south of the equator.

In summary, in the region of the equatorial Pacific, the assimilation integration has a more realistic thermocline structure than the control (Fig. 1) but its model component is not in dynamical balance (Figs. 2 and 3), it has unrealistically large annual mean and monthly mean vertical velocities near 250 m depth (Figs. 4, 5 and 6) and its equatorial undercurrent is less realistic than that of the control integration (Figs. 7 and 8).

3. Physical Discussion and Motivation for Proposed Method

3.1 Dynamical response to imposed density increments

The schematic shown in Fig. 9 suggests how assimilation of thermal data near the equator results in such large vertical velocities and accumulated thermal increments. It depicts the changes in the North-South direction to a state, initially in dynamical balance, which result from decreasing the density of the water (step 1) at some depth. Because of hydrostatic balance the pressure relative to the surroundings will increase above this depth and/or decrease below it (step 2). Assuming that the dynamical response is **not** dominated by the Coriolis acceleration (see next paragraph) the high pressure above the region of lower density will drive a divergent horizontal flow and the low pressure below will drive a convergent horizontal flow. As the 3D flow in the ocean model is non-divergent these horizontal flows drive upward vertical motion through the region where the density was decreased (step 3). The ocean is stably stratified so upward vertical motion will increase the density of the water and hence **oppose the density change which induced the circulation**.

The direct response to density assimilation increments just described is qualitatively accurate for any high-frequency inertia-gravity waves generated. It is not qualitatively correct for any planetary waves generated at mid-latitudes. Near the equator it is not quite clear whether it is relevant to planetary waves; this point was one of the motivations for the analysis presented in section 5.

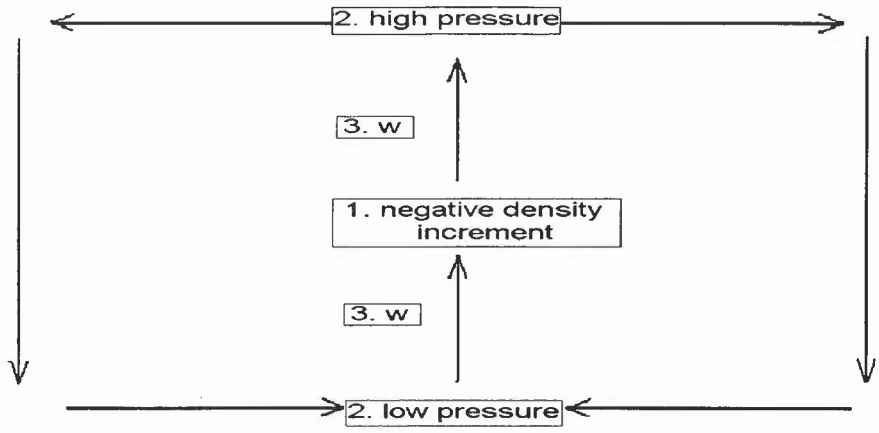

Figure 9: Schematic of the dynamical response to an imposed density increment. Numbers correspond to the steps described in the text of Section 3.1.

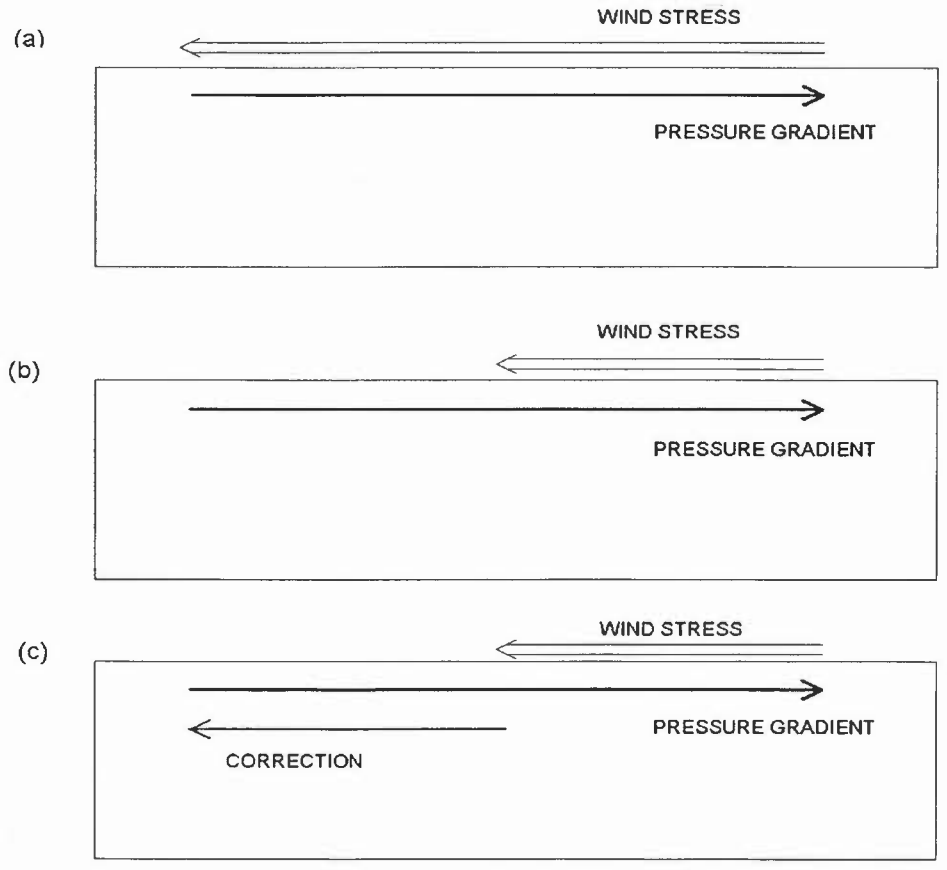

Figure 10: Schematic of the main dynamical balance along the equator between the surface wind stress and pressure gradient: (a) reality, (b) data assimilation and (c) pressure correction.

3.2 Origin of systematic error

The schematic in Fig. 10(a) illustrates the main dynamical balance along the equator which is between the wind stress and the pressure gradients. In normal years easterlies blow along the equator in the Pacific. The surface wind stress is mixed down only over the top 50-100m of the ocean and to oppose this stress by a suitable near-surface pressure gradient the surface of the ocean tilts so that it is higher in the west than the east. This pressure gradient reduces markedly with depth because the water on the eastern side of the Pacific in the upper ocean is colder than that on the western side. In El Nino years the easterly wind stresses are weaker and the surface pressure gradients and sub-surface density gradients weaken to maintain the overall balance.

Figure 10(b) illustrates the way in which data assimilation disrupts this balance in the case when the wind stress driving the ocean model is too weak. In this case assimilation increments to the density field over-strengthen the subsurface pressure gradient. Similarly unbalanced pressure gradients could result if the parametrisation of the downward vertical mixing of momentum input by the wind stress were flawed. Equatorial ocean models were enormously improved by Pacanowski & Philander's (1981) parametrisation of this process. But as the parametrisation of this process is very difficult it is likely to have significant residual errors. Also, if the salinity gradients in the model are incorrect, assimilation of temperature data in some regions may, perhaps after some initial improvement, increase rather than decrease the errors in the density gradients. In such a case assimilation of temperature data would again set off vertical motions.

4. Formulation of Method

4.1 Augmented state treatment of models with systematic errors

For models containing systematic errors, a standard approach is to augment the model state with a set of systematic model error variables (Friedland 1969 and DDS). This section presents the main ideas involved in this approach. The notation is based, wherever possible, on Ide et al. (1997).

The evolution of the true state of the ocean, $\mathbf{x}_k^t \in \mathbb{R}^n$, from time t_k to t_{k+1} is taken to be described by the stochastic vector difference equation

$$\mathbf{x}_{k+1}^t = M^t(\mathbf{x}_k^t, \mathbf{u}_k^t) + \boldsymbol{\eta}_k^t, \qquad (1)$$

where superscript t represents true fields, $M^t : \mathbb{R}^n \times \mathbb{R}^m \to \mathbb{R}^n$ is the true system operator, $\mathbf{u}_k^t \in \mathbb{R}^m$ is the vector of true model inputs (such as the surface wind stress) and $\boldsymbol{\eta}_k^t \in \mathbb{R}^n$ is a vector of random disturbances, assumed to form a white Gaussian sequence.

The observations are assumed to be given by the equation

$$\mathbf{y}_k = H_k(\mathbf{x}_k^t) + \boldsymbol{\varepsilon}_k, \qquad (2)$$

where $\mathbf{y}_k \in \mathbb{R}^{p_k}$ is the vector of observations available at time t_k which is related to the true state of the system through the observation operator $H_k : \mathbb{R}^n \to \mathbb{R}^{p_k}$ and contains random errors $\boldsymbol{\varepsilon}_k \in \mathbb{R}^{p_k}$ which are assumed to form a white Gaussian sequence.

The equation which models the system can be written as

$$\mathbf{x}_{k+1} = M^m(\mathbf{x}_k, \mathbf{u}_k) + \boldsymbol{\eta}_k^m, \tag{3}$$

where superscript m represents model fields, $M^m : \mathbb{R}^n \times \mathbb{R}^m \to \mathbb{R}^n$ is the model system operator and $\boldsymbol{\eta}_k^m \in \mathbb{R}^n$ is a vector of random disturbances, assumed to form a white Gaussian sequence.

It is usually assumed that the forecast model is deterministic, $\boldsymbol{\eta}_k^m \equiv 0$; is perfect, $M^m \equiv M^t$; and has perfect inputs, $\mathbf{u}_k \equiv \mathbf{u}_k^t$. In this case, the normal data assimilation process may be applied and the analysed solution can be made to converge to the true solution over time by suitable choices of the gain matrix, given certain conditions. For ocean models, these assumptions about the forecast model are not valid. This is also true for many other applications such as humidity fields in NWP. When modelling systems such as the oceans, the exact representation of the true system on the model grid will not be known, and approximations to the true operator have to be made. Also, the inputs to the model are not always known accurately.

We now suppose instead that the model used to propagate the state variables and inputs contains systematic errors. We write this assumption as

$$M^m(\mathbf{x}_k, \mathbf{u}_k) = M^t(\mathbf{x}_k, \mathbf{u}_k) + T(\mathbf{b}_k), \tag{4}$$

where $\mathbf{b}_k \in \mathbb{R}^q$ and $T : \mathbb{R}^q \to \mathbb{R}^n$ is some operator which is to be chosen. The vector $\mathbf{b}_k$ is not strictly the systematic model error vector after introducing the operator T. However, we call this vector the model bias in this section for convenience. The operator is included because it is possible that only certain parts of the model will contain systematic errors, i.e. $q < n$. T is usually taken to be the identity as in DDS but there are other possible choices. In the pressure correction method described in the following subsection, we take the operator T to be of a specific form, based on our understanding of the nature of the systematic errors.

We assume that the evolution of the model biases is governed by the stochastic vector difference equation

$$\mathbf{b}_{k+1} = W(\mathbf{b}_k, \mathbf{x}_k) + \zeta_k, \tag{5}$$

where $W : \mathbb{R}^q \times \mathbb{R}^n \to \mathbb{R}^q$ evolves the model bias variables and $\zeta_k \in \mathbb{R}^q$ forms a white Gaussian sequence.

If the normal data assimilation process is applied to the system with systematic model errors, the analysed solution will not converge to the true solution as time increases. If we augment the state vector with the vector of model bias variables and apply the data assimilation process to this augmented state however, then it can be shown in the linear case that the analysed state

vector can be made to converge to the true state vector, given similar conditions to those for the normal data assimilation problem. This convergence assumes that we know how the systematic model error evolves in time.

The idea of state augmentation can be applied to any of the data assimilation methods. In the case of Optimal Interpolation, the analysis step can be written as

$$\mathbf{x}_k^a = \mathbf{x}_k^f + \mathbf{K}_k^x[\mathbf{y}_k - H_k(\mathbf{x}_k^f)], \tag{6}$$

$$\mathbf{b}_k^a = \mathbf{b}_k^f + \mathbf{K}_k^b[\mathbf{y}_k - H_k(\mathbf{x}_k^f)], \tag{7}$$

where the gain matrices are determined by

$$\mathbf{K}_k^x = \mathbf{P}_{(xx)}^f(t_k)\mathbf{H}_k^T[\mathbf{H}_k\mathbf{P}_{(xx)}^f(t_k)\mathbf{H}_k^T + \mathbf{R}_k]^{-1}, \tag{8}$$

$$\mathbf{K}_k^b = \mathbf{P}_{(xb)}^{fT}(t_k)\mathbf{H}_k^T[\mathbf{H}_k\mathbf{P}_{(xx)}^f(t_k)\mathbf{H}_k^T + \mathbf{R}_k]^{-1}. \tag{9}$$

Here, $\mathbf{P}_{(xx)}^f(t_k) \in \mathbb{R}^{n\times n}$ is the forecast error covariance matrix for the state variables, $\mathbf{P}_{(xb)}^f(t_k) \in \mathbb{R}^{q\times n}$ is the cross-covariance matrix between errors in the state and errors in the model bias variables, $\mathbf{H}_k \in \mathbb{R}^{p_k\times n}$ is the linearised observation operator and $\mathbf{R}_k \in \mathbb{R}^{p_k\times p_k}$ is the observation error covariance matrix.

As well as converging to the true state vector, a potential advantage of this method is that we obtain an estimate of the errors in the model which might help to improve its weaker components. A difficulty of the method is that we may not know exactly how the systematic model errors evolve. If we can make a reasonable estimate, however, the analysis of the augmented state should provide a better analysis than that without the systematic model error correction.

4.2 The pressure correction method

We now introduce specific choices for $\mathbf{K}_k^b$, T and W for the bias correction, aimed at reducing the effects of the systematic errors described in sections 3.1 and 3.2, that is to restore the balance between the surface wind stress and the model's pressure gradients. We assume that we have observations of potential temperature and salinity only, and use these observations to produce bias fields which will correct the model's pressure gradients.

In the normal data assimilation procedure, increments to the potential temperature and salinity fields are made using the differences between the observed and model forecast fields. To produce estimates of the bias in these model fields, an analysis of the form of Eq. (7) is performed, i.e.

$$\theta_k^{b\,a} = \theta_k^{b\,f} + \mathbf{K}_k^{b\,\theta}[\theta_k^o - H_k^\theta(\theta_k^f)], \qquad \mathbf{S}_k^{b\,a} = \mathbf{S}_k^{b\,f} + \mathbf{K}_k^{b\,S}[\mathbf{S}_k^o - H_k^S(\mathbf{S}_k^f)], \tag{10}$$

where θ_k and S_k are the potential temperature and salinity respectively at time t_k, superscript b indicates a bias field, superscript a indicates analysis, superscript f indicates forecast, superscript o denotes observations, H_k^θ interpolates from the model grid to the temperature

observations' positions and H_k^S interpolates from the model grid to the salinity observations' positions.

The forecast model of θ_k^b and $\mathbf{S}_k^b$ is assumed in this paper to be constant, so that

$$\theta_{k+1}^{bf} = \theta_k^{ba}, \qquad S_{k+1}^{bf} = S_k^{ba}, \tag{11}$$

although this can be altered if something is known about how the bias fields evolve. Initially, the temperature and salinity bias fields are set to zero, i.e. $\theta_0^{ba} = S_0^{ba} = 0$.

The expression for the gain matrix for the bias variables written in Eq. (9) involves the cross-covariance matrix for the errors in the state and model bias variables. Statistics for this calculation would be very difficult to obtain so we choose this matrix to be of a simple form,

$$\mathbf{K}_k^b = -\alpha \mathbf{K}_k^x, \tag{12}$$

where α is a constant between zero and one.

The estimates of the biases in the temperature and salinity fields described in Eq. (10) should now be used to calculate a bias in the pressure field so that the balance described in section 3.2 between the pressure gradient and wind forcing can be restored. This is done by making use of the operator T in Eq. (4), so that the bias fields are not simply added onto the model equations. Instead, a biased density ρ_k^b is calculated through the equation of state,

$$\rho_k^b = \rho(\theta_k^{ma} + \theta_k^{ba}, \mathbf{S}_k^{ma} + \mathbf{S}_k^{ba}) - \rho_k^m, \tag{13}$$

and this is used through the hydrostatic equation to produce a compensating model "pressure" field,

$$p_k^b(z) = \int_{-H}^{z} -\rho_k^b g dz. \tag{14}$$

where z is depth, H is the depth of the ocean and g is the gravitational constant. The pressure at the bottom of the model is kept the same during this calculation. Also, the model's potential temperature and salinity fields are not altered during this operation.

The corrected pressure field is now used in the horizontal momentum equations which can be written in the continuous case as

$$\partial u^m / \partial t + \Gamma(u^m) - f v^m = -\partial(p^m + p^b)/\partial x + \partial \tau_{xz}/\partial z, \tag{15}$$

$$\partial v^m / \partial t + \Gamma(v^m) + f u^m = -\partial(p^m + p^b)/\partial y + \partial \tau_{yz}/\partial z, \tag{16}$$

where (x, y) and (u, v) are the eastward and northward coordinates and velocities respectively, (τ_x, τ_y) are the corresponding components of the wind forcing and Γ represents an advective operator. The extra pressure gradient terms on the right hand side of these equations will act in

the opposite sense to the pressure gradients resulting from the nomal assimilation increments. Where the response of the model was to oppose the assimilation in the original scheme, the relatively small bias correction increments to the pressure field will slowly build up until they are of significant amplitude. The resulting pressure gradients will oppose those imposed by the original assimilation increments as in Fig. 10(c), restore the balance between the pressure gradients and the surface wind stresses, and hence prevent or at least dampen spurious circulations. Where the model responds "positively" to the assimilation, re-inforcing its increments, the time-mean assimilation increments will be small and the response to the additional pressure field insignificant.

The compensating field p^b is referred to as a pressure correction because it is a scalar field which is related to the temperature and salinity bias fields (11) through the density and hydrostatic equations (13) and (14). Strictly speaking however, when the main errors in the model system are in the wind stresses driving it, the vertical distribution of these momentum inputs into the model (as discussed in section 3.2) $\partial p^b / \partial x$ in (15) should be interpreted as a correction to $\partial \tau_{xz} / \partial z$ rather than the pressure gradient $\partial p^m / \partial x$.

As the pressure correction method only changes the pressure field in the model's horizontal momentum equations, it is fairly clear that systematic errors in the wind stress curl will not be "corrected" by the technique; i.e. the model will not converge to the true solution when there is a time independent error in the wind stress curl (see sub-section 5.2). In mid-latitudes it is arguably an advantage to use a pressure correction field which will generate mainly geostrophic and non-divergent velocities. Also it may be that when only observations of tracers and surface height are assimilated a suitably chosen scalar correction field is sufficient to dampen any unphysical motions generated. This topic is discussed further in section 6.

5. Convergence and stability analysis for method applied to Shallow Water Equations

Much understanding of equatorial dynamics can be gleaned from consideration of small amplitude motions superimposed on a horizontally uniform stratified state at rest in a flat bottomed ocean (Gill, 1980, 1982). Each internal mode of motion can be considered separately and is governed by the shallow water equations (SWEs) in which the effective depth H_e depends on the vertical mode number (Gill 1982) and the surface height, η, corresponds to the amplitude of the density perturbation in this vertical mode. Thus the analysis of the SWEs is very relevant to the assimilation of observations of ocean density near the equator.

Davies & Turner (1977) presented some analytical results on the convergence of SWE models to the true solutions when fields of temperature and pressure data alone are nudged into them. Section 12.8 of Daley (1991) provides a useful summary of results on a f-plane. To make the algebra tractable full fields of subsets of the model fields are assumed to be available for assimilation and are simply nudged pointwise into the model fields. Here we suppose that the wind stress forcing is in error and that the model equations are otherwise perfect.

In sub-section 5.1 the pressure correction method is applied to the SWEs and a set of equations is derived for the evolution of the errors in the model fields. The following sub-sections analyse the solutions of this set of equations on the equatorial β-plane. Stationary solutions for stationary forcing are discussed in 5.2 then the energetics in 5.3. The dispersion relation for solutions in the

absence of forcing is derived in 5.4 and analysed for the pair of roots corresponding to gravity waves in 5.5. Results for planetary and Kelvin waves are stated in 5.6. The additional set of slow wave solutions arising from the new variable, h, is considered in 5.7. In order to complete the analysis, particular solutions with time dependent forcing by errors in the wind stress are required. These can be constructed using the ladder operators exploited in Gill (1980) but the details are not presented here.

The analysis of the solutions for an f-plane is a simple extension of section 12.8 of Daley (1991). The solutions for stationary forcing differ significantly from those for the β-plane (see sub-section 5.2). As the solutions for a f-plane have a curious character and are of little relevance to the problems described in section 2 they are omitted.

5.1 Statement of pressure correction equations

As is standard in control theory methods, we write down the model equations with the model variables denoted by a superscript m and suppose that a related set of equations holds for the true fields which are denoted by the superscript t. The true fields are thus supposed to satisfy:

$$\partial u^t/\partial t - fv^t = -g\partial\eta^t/\partial x + \tau_x^t \quad , \tag{17}$$

$$\partial v^t/\partial t + fu^t = -g\partial\eta^t/\partial y + \tau_y^t \quad , \tag{18}$$

$$\partial\eta^t/\partial t + H_e(\partial u^t/\partial x + \partial v^t/\partial y) = 0 \quad , \tag{19}$$

where f is the Coriolis parameter. Equations (17) and (18) are the eastward and northward components of the momentum equations and (19) is the continuity equation. We will set $f = \beta y$, which is a good approximation near the equator.

The equations governing the evolution of the model as it assimilates full fields of surface height data using a nudging method with the pressure correction method are:

$$\partial u^m/\partial t - fv^m = -g\partial/\partial x(\eta^m + h) + \tau_x^m \quad , \tag{20}$$

$$\partial v^m/\partial t + fu^m = -g\partial/\partial y(\eta^m + h) + \tau_y^m \quad , \tag{21}$$

$$\partial\eta^m/\partial t + \varepsilon(\eta^m - \eta^t) + H_e(\partial u^m/\partial x + \partial v^m/\partial y) = 0 \quad , \tag{22}$$

$$\partial h/\partial t - \gamma(\eta^m - \eta^t) = 0 \quad . \tag{23}$$

Here h is the surface height correction field ("the pressure correction" field for this model). Full fields of surface height are assimilated into the model using a nudging coefficient ε in (22). Similar assimilation increments proportional to $\eta^m - \eta^t$ are made to h, but with coefficient $-\gamma$. We will take $\gamma, \varepsilon > 0$ and $\gamma < \varepsilon$.

Denoting the difference between the model and true fields without superscripts,

$$\psi^m - \psi^t = \psi \quad for \quad \psi = u, v, \eta, \tau_x, \tau_y, \tag{24}$$

and subtracting (17)-(19) from (20)-(22) respectively one obtains

$$\partial u/\partial t - fv = -g\partial/\partial x(\eta + h) + \tau_x \quad , \tag{25}$$

$$\partial v/\partial t + fu = -g\partial/\partial y(\eta + h) + \tau_y \quad , \tag{26}$$

$$\partial \eta/\partial t + \varepsilon\eta + H_e(\partial u/\partial x + \partial v/\partial y) = 0 \quad , \tag{27}$$

$$\partial h/\partial t - \gamma\eta = 0 \quad . \tag{28}$$

5.2 Stationary solutions for stationary forcing

When $\gamma \neq 0$, (28) implies that $\eta=0$ for any stationary solution and (27) then implies that $\partial u/\partial x+\partial v/\partial y=0$. For the 3D problem mentioned at the start of the section this implies that the vertical velocity is zero. Thus when the pressure correction method is used the stationary solutions for the density, pressure and vertical velocity fields all match those of the true solution even when the solution is driven by incorrect wind stresses. This is to be contrasted with the stationary solutions obtained in the absence of pressure correction ($\gamma=0$) for which none of these fields match the true solution

When $\gamma \neq 0$, the curl of (25) and (26) determines the error in the northward velocity driven by the error in the wind forcing:

$$-\beta v = \partial \tau_y/\partial x - \partial \tau_x/\partial y \quad . \tag{29}$$

$\partial u/\partial x+\partial v/\partial y=0$ then determines $\partial u/\partial x$ and prescribing $u=0$ at the eastern boundary fixes u. The divergence of (25) and (26) gives an elliptic problem for h,

$$g(\partial^2/\partial x^2 + \partial^2/\partial y^2)h = f(\partial v/\partial x - \partial u/\partial y) + \partial \tau_x/\partial x + \partial \tau_y/\partial y \quad , \tag{30}$$

which can be solved using boundary conditions on the normal derivative of h.

5.3 Energetics

An energy equation for (17)-(18) can be derived:

$$\begin{aligned} &\tfrac{1}{2}\partial/\partial t\left\{H_e(u^2+v^2) + g(\eta+h)^2 + \tfrac{1}{2}g\frac{(\varepsilon-\gamma)}{\gamma}h^2\right\} = \\ &\quad H_e\mathbf{u}.\boldsymbol{\tau} - gH_e\nabla_h.[\mathbf{u}(\eta+h)] - g(\varepsilon-\gamma)\eta^2 \quad . \end{aligned} \tag{31}$$

The first term on the r.h.s. of (31) is the work done by the wind stress. The second term is a flux which given suitable boundary conditions is zero for the domain integral of the energy. The third term is a sink of energy. The last term on the l.h.s. can be viewed as an additional term in the energy, the energy of the pressure correction field. In the absence of wind forcing this energy norm must decrease until η and hence h is zero everywhere. The important point is that there are no spurious sources of energy.

5.4 Dispersion relation for homogeneous solutions

Various methods can be used to eliminate u, η and h from (25)-(28) to find a single equation for v:

$$\frac{1}{c_e^2}\partial/\partial t\left(\partial/\partial t+\varepsilon\right)\left(\partial^2 v/\partial t^2+f^2 v\right)-\left(\partial/\partial t+\gamma\right)\left(\nabla_h^2\partial v/\partial t+\beta\partial v/\partial x\right)=0 \quad . \qquad (32)$$

See Appendix A for an outline of a derivation. Equatorially trapped solutions of (32) which are periodic in *x* can be sought in the form

$$v=\hat{v}(y)\exp i(kx-\omega t) \quad . \qquad (33)$$

Four solutions should be obtainable for each k They decay to zero if and only if the imaginary part of ω is negative. By introducing a change of variable for y one can re-cast (32) into a standard form. The new variable is complex-valued so we denote it by Z. With the following choice Z is non-dimensional

$$y=\alpha Z \quad , \qquad (34)$$

$$\alpha^4=\frac{c_e^2}{\beta^2}\left(\frac{\omega+i\gamma}{\omega+i\varepsilon}\right) \quad . \qquad (35)$$

(32) can then be re-written in the standard form

$$d^2\hat{v}/dZ^2-Z^2\hat{v}+\lambda\hat{v}=0, \qquad (36)$$

$$\alpha^2\beta^2\lambda=\omega^2-\alpha^4\beta^2(k^2+\beta k/\omega) \quad . \qquad (37)$$

As Z^2 is an analytic function, (36) is satisfied in the complex Z plane by its analytic function solutions. The standard solutions,

$$\hat{v}=\exp(-Z^2/2)H_n(Z) \quad , \quad \lambda=2n+1 \quad , \quad n=0,1,2,... \quad , \qquad (38)$$

where H_n is the nth order Hermite polynomial, are bounded as $|y|\to\infty$, provided Re{α^2 }> 0. If Re{α^2 }< 0, the solutions which are bounded as $|y|\to\infty$ are

$$\hat{v}=v_0\exp(Z^2/2)I_n(Z) \quad , \quad -\lambda=2n+1 \quad , \quad n=0,1,2,... \quad . \qquad (39)$$

Equations (35), (37) and (38) or (39) together define ω.

Solutions for ω are sought below assuming that the timescales of ε and/or γ are slow compared with the timescales which otherwise determine ω. The typical values of the dimensional parameters involved in the problem are $\beta=2\times10^{-11}m^{-1}s^{-1}$, $c_e=3ms^{-1}$, and $k=10^{-6}m^{-1}$. Combinations of these which have the units of a frequency are $\beta/k=2\times10^{-5}s^{-1}$, $(\beta/c_e)^{1/2}=8\times10^{-6}s^{-1}$ and $kc_e=3\times10^{-6}s^{-1}$. The non-dimensional ratio

$$r = \frac{(2n+1)\beta c_e}{(kc_e)^2} \simeq 6(2n+1). \qquad (40)$$

is an important quantity. In practice r is quite large, particularly for long zonal wavelengths and large values of n. The assimilation scheme described in section 2 uses a time window of 10 days (on either side of each observation) and the rate $\varepsilon \simeq 1/10\,day^{-1} = 10^{-6}s^{-1}$. ε will be considered to be a small quantity relative to these other quantities or to the frequency ω_0 of the original solution i.e. $\varepsilon/\omega_0 \ll 1$. The rate γ is expected to be 3 to 10 times smaller than ε. Thus it is more relevant to take γ to be the only small quantity in some cases.

5.5 Gravity wave solutions

The standard approximation to the dispersion relation for gravity waves is to neglect the term $\beta k/\omega$ on the r.h.s. of (37). Using (38) the dispersion relation is:

$$\omega^2 = \alpha^4\beta^2k^2 + (2n+1)\alpha^2\beta^2 \quad . \qquad (41)$$

When $\varepsilon = \gamma = 0$ the solution has

$$\omega_0^2 = (kc_e)^2 + (2n+1)\beta c_e = (kc_e)^2(1+r) \quad . \qquad (42)$$

Writing $\omega = \omega_0 + \omega_1 + \ldots$ with $\omega_1 = O(\varepsilon)$ we expand (41) about the solution (42). To simplify the algebra we introduce δ defined by

$$(1+\delta) \equiv \alpha^2\beta/c_e \quad . \qquad (43)$$

The dependence of δ on ω_1 will be calculated shortly (in (45)). Substituting (42) and (43) into (41) one obtains

$$2\omega_0\omega_1 = \delta(kc_e)^2(2+r). \qquad (44)$$

From the definitions (28) and (36)

$$(1+\delta)^2 = \frac{\omega+i\gamma}{\omega+i\varepsilon} \Rightarrow 2\delta_i = \frac{-(\omega_0+\omega_{1r})(\varepsilon-\gamma)}{(\omega_0+\omega_{1r})^2+(\varepsilon+\omega_{1i})^2} \quad . \qquad (45)$$

where the subscripts r and i indicate the real and imaginary parts of a quantity respectively and the second equality is the imaginary part of the first equality. Thus combining (44) and (45):

$$4\omega_{1i} = -(\varepsilon-\gamma)\frac{(2+r)}{(1+r)} \quad . \qquad (46)$$

In the absence of any forcing the gravity waves decay towards the true gravity waves at a rate within a factor of 2 to 4 of $\varepsilon-\gamma$.

5.6 Planetary and Kelvin wave solutions

For planetary waves the standard approximate form of the dispersion relation neglects the term equal to ω^2 on the r.h.s. of (37). A very similar calculation to that for gravity waves gives

$$\omega_0 = \frac{-\beta/k}{(1+r)} \qquad \text{and} \qquad \omega_{1i} = -\frac{r}{r+1}\frac{\varepsilon-\gamma}{2} \quad . \tag{47}$$

Note that the assumption $\varepsilon/\omega_0 \ll 1$ is unlikely to be realistic for moderately large values of r.

It is characteristic of Kelvin waves that v=0. The component of the momentum equation parallel to the equator and the continuity equation determine the motion and seeking solutions periodic in *x* and *t* as before one finds:

$$(-i\omega+\varepsilon)\omega^2 = k^2c_e^2(-i\omega+\gamma) \quad . \tag{48}$$

There are three roots which for small ε and γ tend to ω_0=0 and $\omega_0^2 = (kc_e)^2$. The root $\omega_0 = -kc_e$ is excluded because its solution is not bounded for $|y| \to \infty$. The root with $\omega_0 = kc_e$ for small ε and γ has ω_{1i} given by (46) with r=0. The root ω_0=0 is discussed in detail in the next sub-section.

5.7 Additional slow wave solution

When $\varepsilon = \gamma = 0$, $\eta + h = u = v = 0$ is a solution with $\omega = 0$. We will explore this solution for small values of γ assuming that $\varepsilon = O(1)$. To find the structure of the solution it is necessary to work through several orders in γ of the dispersion relation. It transpires that it is best to work with the full dispersion relation (37). After squaring and using the definition of α in (35), (37) can be written in the form:

$$\begin{aligned}\lambda^2(\omega+i\varepsilon)(\omega+i\gamma)\omega^2\beta^2c_e^2 &= \omega^6(\omega+i\varepsilon)^2 \\ &-2\omega^3c_e^2(\omega+i\varepsilon)(\omega+i\gamma)k(\omega k+\beta)+c_e^4(\omega+i\gamma)^2k^2(\omega k+\beta)^2 \quad .\end{aligned} \tag{49}$$

Writing $\omega = \omega_1 + \omega_2 + \omega_3 + \ldots$ where ω_n is of O(γ^n), and assuming that βc_e and $(kc_e)^2$ are of similar magnitudes to $O(\beta^2c_e^2\gamma^2)$ (49) gives

$$\omega_1 = -i\gamma \quad . \tag{50}$$

Thus this root decays at the rate $1/\gamma$. To find the structure of the solution we examine (49) next to $O(\beta^2c_e^2\gamma^4)$ which gives

$$\lambda^2 i\varepsilon\omega_2(-i\gamma)^2\beta^2c_e^2 = c_e^4\omega_2^2\beta^2k^2 \quad \Rightarrow \omega_2 = \frac{-i\lambda^2\varepsilon\gamma^2}{k^2c_e^2} \quad . \tag{51}$$

To this order the solution does not decay away from the equator because

$$\alpha^4 = \frac{c_e^2}{\beta^2}\left(\frac{\omega+i\gamma}{i\varepsilon}\right) \quad = \quad -\frac{\lambda^2\gamma^2}{k^2c_e^2} \quad , \tag{52}$$

so α^2 is a pure imaginary number and (38) and (39) describe functions oscillating in y like $\exp\left(ikc_e y^2/\lambda\gamma\right)$. To find the scale on which the function decays to zero (49) must be examined to the next order $O\left(\beta^2c_e^2\gamma^5\right)$ which gives:

$$\omega_3 = \frac{-2\varepsilon\gamma^3}{\beta kc_e^2}\left\{\lambda^2-1\right\} - \frac{i\gamma^3\lambda^2}{k^2c_e^2}\left\{1+\frac{\lambda^2\varepsilon^2}{k^2c_e^2}\right\} \quad . \tag{53}$$

Note that $\omega_{3r} = 0$ for the mode with $n = 0$. Except for this case to $O(\gamma^3)$

$$\alpha^4 = \frac{c_e^2}{\beta^2}\left(\frac{\omega+i\gamma}{\omega+i\varepsilon}\right) = \frac{i\omega_{2i}+\omega_3}{i(\varepsilon-\gamma)} = \frac{\omega_{2i}}{(\varepsilon-\gamma)} - \frac{i\omega_3}{\varepsilon} \equiv -p_1^2\gamma^2(1+ip_2\gamma) \tag{54}$$

where p_1 and p_2 are positive constants of O(1).

The value of α^4 is the same whether solutions (38) or (39) are being calculated because only λ^2 appears in (49). For each solution only one choice for the sign of the square root of α^4 will satisfy (37). From the position of λ in (37) it is clear that α^2 will be the same for both solutions (38) and (39). Then if $\mathrm{Re}\{\alpha^2\} > 0$ solution (38) will be bounded and if $\mathrm{Re}\{\alpha^2\} < 0$ solution (39) is the relevant bounded one. The meridional structure of the solution is of the form

$$\exp\frac{-y^2}{\alpha^2} = \exp\frac{-y^2}{-ip_1\gamma(1+ip_2\gamma/2)} \simeq \exp\frac{-iy^2}{p_1\gamma}\exp\frac{-p_2y^2}{2p_1} \quad . \tag{55}$$

6. Discussion

The pressure correction method has some similarities with the assimilation of anomalies from climatology. It is simplest to discuss this in terms of the SWEs as studied in section 5. The observational increments in the anomaly assimilation scheme are given by

$$\Delta\eta = (\eta^t - \overline{\eta}^t) - (\eta^m - \overline{\eta}^m), \tag{56}$$

where the overbar indicates climatology. Thus the equations for the climate anomaly assimilation scheme corresponding to (20)-(22) are

$$\partial u^m/\partial t - fv^m = -g\partial\eta^m/\partial x + \tau_x^m, \quad (57)$$

$$\partial v^m/\partial t + fu^m = -g\partial\eta^m/\partial y + \tau_y^m, \quad (58)$$

$$\partial\eta^m/\partial t + \varepsilon(\eta^m - \overline{\eta}^m - \eta' + \overline{\eta}') + H_e(\partial u^m/\partial x + \partial v^m/\partial y) = 0. \quad (59)$$

Following DDS let an unbiased estimate of the surface height be denoted by $\tilde{\eta}^m$. For the climate anomaly scheme $\tilde{\eta}^m = \eta^m + \overline{\eta}' - \overline{\eta}^m$. Writing $\overline{h} = \overline{\eta}^m - \overline{\eta}'$ and assuming that $\overline{h}$ is independent of time one obtains

$$\partial u^m/\partial t - fv^m = -g\partial/\partial x(\tilde{\eta}^m + \overline{h}) + \tau_x^m, \quad (60)$$

$$\partial v^m/\partial t + fu^m = -g\partial/\partial y(\tilde{\eta}^m + \overline{h}) + \tau_y^m, \quad (61)$$

$$\partial\tilde{\eta}^m/\partial t + \varepsilon(\tilde{\eta}^m - \eta') + H_e(\partial u^m/\partial x + \partial v^m/\partial y) = 0, \quad (62)$$

which is identical to (20)-(22) when $\tilde{\eta}^m = \eta^m$ and $\overline{h} = h$. Thus the climate anomaly and pressure correction schemes are formally identical. There are however two important differences between the two schemes. Firstly, the pressure correction method builds up the correction field interactively whilst assimilating data and so can respond to any changes in the model biases. Secondly, the surface height and tracer fields in the pressure correction method will converge to the true fields whereas those of the climate anomaly scheme will converge to biased fields (whose climatological means equal those of the model integrated without data assimilation). This is an advantage for the pressure correction when it is applied to coupled ocean-atmosphere models because its surface temperature analyses will be unbiased and hence suitable for interaction with the atmosphere model.

The three bias correction methods summarised in section 5(b) of DDS all differ from our method of pressure correction. Their final method, "on-line estimation with feedback", appears to be closest to our scheme conceptually but in their formulation the bias field for the change over one time-step of the surface height, h, is added directly as a correction to the surface height field. Hence, if the data assimilation is univariate and only surface height data are assimilated, their scheme will only make a bias correction to the evolution equation (59) for the surface height whereas the pressure correction scheme would amend only the momentum equations (57) and (58). Their other "on-line" method appears at first to be similar to an "interactive" form of the anomaly assimilation given by (57)-(59) in that the forecast model uses a biased state vector (DDS (100)) as in (57) and (58) but the analysis step (DDS (105)) draws the biased state towards the true state (as in (62)) rather than towards a biased state (as in (59)).

For seasonal forecasting with coupled models, appropriate specification of the decay of the pressure correction field during the forecast period will be necessary to reap much benefit from the pressure correction scheme. The best approach will depend on the way in which the analysis stage has been performed. If the surface fluxes used in the analysis stage do not originate from the atmospheric model used in the coupled forecasts, the biases in the two stages will probably have different characteristics. In this case, the bias field should be decreased to zero fairly rapidly in the forecast. The only advantage obtained by using the pressure correction method would be that the initial analyses are more balanced and so the model may take slightly longer than previously to drift to the biased state given by the new forcing fluxes. If the atmospheric model used in the coupled system supplies the surface fluxes during the analysis then the model biases are more likely to be similar in both stages, though assimilation of data into the atmospheric model could clearly alter the characteristics of its biases. Even if no data is assimilated into the

atmospheric model, the bias field is still likely to vary significantly over seasonal timescales and should probably be allowed to decay towards zero over a period of 3-12 months.

This paper has only discussed assimilation of temperature and salinity observations. The extension of the method for use with the large amount of altimeter data which is currently available is an area for future work. These data would be important for the application of the pressure correction method away from the equator, especially in the western boundary currents where coarse resolution models have significant biases. It may also be useful to attempt to estimate biases in the horizontal component of the stress tensor which has non-zero curl. Equation (29) suggests that it may be possible to use northward velocity observations to make corrections to this component. The application of the pressure correction method to more sophisticated data assimilation methods, such as the various approximations of the Kalman filter, is another area which might be examined in the future. The ideas presented here might also be adapted for use in atmospheric models with significant biases near the equator.

7. Concluding summary

It has been shown that simple assimilation of thermal profile data from the equatorial Pacific (e.g. the TAO array of moorings) into an ocean general circulation model can result in unrealistically strong vertical motions (figures 4-5) near the equator which counteract some of the increments made by the data assimilation scheme and lead to similar increments to the model state being repeatedly made by the assimilation scheme (figures 2-3). Figure 9 illustrates the "equatorial bonfire" dynamics of the response of an ocean model to unbalanced density increments near the equator. Figure 10 illustrates and section 3.2 discusses how difficulties in representing the momentum balance in the equatorial oceans can lead to an ocean state with a biased density field and hence unbalanced density assimilation increments.

Section 4.1 outlines the general theory of augmenting a model's state vector by a bias state vector and estimating the bias state vector by data assimilation methods (see particularly (7) and (9)). The pressure correction method is presented in section 4.2 (equations (10)-(16)) as an application of the general theory which, motiviated by the dynamics discussed above, makes specific choices for estimates of the covariances between errors in the model state and the model bias. In particular it assumes that the biases in the model equations are confined to the momentum equations and amends them only by addition of a pressure gradient bias field. Section 5 analyses the characteristics of the method when it is applied to the shallow water equations on a β-plane with incorrect windstresses driving the model and full fields of surface height available for assimilation. The model errors are shown to evolve according to (25)-(28) and the errors in the unforced (gravity, Rossby and Kelvin) waves are shown to decay with time. The first paragraph of section 5.2 establishes that time independent erroneous wind-forcing does not generate erroneous surface height or horizontal divergence fields even when there are errors in the curl of the wind stress. Section 6 relates the method to assimilation of climate anomalies.

Appendix A

Reduction of modified shallow water equations to a single variable

To derive (32) from (25)-(28) we firstly eliminate u. From (25) and (26)

$$\partial^2 v/\partial t^2 + f^2 v = -g\left(\partial^2/\partial y \partial t(\eta + h) - f\partial/\partial x(\eta + h)\right) \equiv -gA \quad . \qquad \text{(A1)}$$

The curl of the momentum equations and the continuity equation also give

$$H_e(\nabla_h^2 \partial v/\partial t + \beta \partial v/\partial x) = -\left(\partial/\partial t + \varepsilon\right)\left(\partial^2 \eta/\partial y \partial t - f\partial \eta/\partial x\right) \equiv -B \quad . \qquad \text{(A2)}$$

From the definitions of A and B introduced in (A1) and (A2), and (19)

$$\partial/\partial t\left(\partial/\partial t + \varepsilon\right) A = \left(\partial/\partial t + \gamma\right) B \quad . \qquad \text{(A3)}$$

Equation (32) may be derived by substituting expressions for A and B from the l.h.sides of (A1) and (A2) into (A3).

Appendix B

Results of applying pressure correction method to FOAM

The integration assimilating data described in section 2 has been repeated using the pressure correction scheme as described in section 4.2. The weighting of the error covariance described in equation (12) is chosen to be (i) $\alpha = 0.1$ and (ii) $\alpha = 0.3$. Figure B1 (a) and (b) show the time mean potential temperature fields for these two integrations in a form which enables direct comparison with the results discussed in section 2. Figure 1(b) and Figs. B1(a) and (b) are generally in quite close agreement – the thermocline still contains the tight temperature gradients - but there are discernible differences particularly below 100 m depth near 90°W. Table B1 presents statistics describing the fit of the analyses to thermal profile observations within 5° of the equator from a three-month period during the second year of integration just before the observations are used (forecast) and at the time of validity of the observations (analysis). The second column of table B1, labelled α=0, presents values for the standard assimilation integration without pressure correction. The values show that the thermal fields from the pressure correction integrations fit the observations more closely at 50 m depth than the standard assimilation. At 200m depth, results from the three integrations are very similar.

The time mean potential temperature increment fields from the three assimilation runs along the equator in the Pacific are shown in Fig. B2. It is clear that the temperature increments are much smaller in magnitude for the runs with the pressure correction included than for the standard integration shown in Fig. 2, and are constrained to the top 150m. The maximum values for the pressure corrected runs are about 2°C per month compared with 4°C per month for the run with normal data assimilation. Figure B3 shows a horizontal view of the temperature increment fields at 50m depth for both the pressure corrected integrations. This shows that the increments are still concentrated near the equator.

	Depth (m)	$\alpha = 0$	$\alpha = 0.1$	$\alpha = 0.3$
Variances of $(\theta^f - \theta^o)$				
	47.85	1.10	0.98	0.85
	203.7	0.72	0.72	0.75
Variances of $(\theta^a - \theta^o)$				
	47.85	1.00	0.88	0.77
	203.7	0.67	0.64	0.68

Table B1. Variances in the region 140°E - 80°W, ±5°N/S of (forecast – observations) and (analysis – observations) of temperature for the period May – July 1996.

In Fig. B4, the annual mean vertical velocities from the second year of integration at 250m depth are presented. The pressure corrected runs both have significantly smaller vertical velocities at this depth than those for the run with normal data assimilation. The magnitude of the velocities in the pressure corrected integrations are now comparable to the control run without data assimilation, though the locations of upwelling and downwelling are different in all four experiments. Figure B5 shows that the large annual mean vertical velocities below 150m depth which were present in the run with normal data assimilation at the 110°W cross section have been eliminated.

Figure B6 presents zonal velocity cross sections along the equator in the Pacific for the pressure corrected integrations. The maximum speed in the equatorial undercurrent and increased eastward penetration of the current in both pressure correction integrations are significant improvements over both the control and standard assimilation integrations. The surface currents are now of similar structure to the control, with the reversal of the surface currents in the run with normal data assimilation having been eliminated. The meridional structure of the horizontal velocities is presented in Fig. B7 (a) and (b) which shows that the general structure of the currents are similar in the pressure corrected runs to the normal assimilation integration, the main differences being a weakening of the main equatorial undercurrent and an extension of the current further to the east.

Figure B8 displays the annual mean bias correction field, $\theta^{b\,a}$, at 50m depth for the second year of integration. The field for α=0.1 has relatively modest values (typically smaller than 2.5°C) and the largest values are within 15° of the equator to the North and South. The bias correction thermal field for α=0.3 has a somewhat similar structure to that for α=0.1 but much larger amplitudes. A vertical cross section of these fields is given in Fig. B9 along the equator. This shows that most of the field is concentrated in the top 200m and is sloping down towards the west, the values being positive above the thermocline and negative below it.

The annual mean pressure correction field, p^b, has been calculated using equations (13) and (14). The gradients of this field in the x and y direction at the surface are shown in Figs. B10 and B11 respectively. These quantities are the mean correction to the momentum equations (15) and (16). This shows a surprising result in that the gradients in the y direction are larger than those in the x direction. This is unexpected because the wind stresses are largely zonal in the equatorial Pacific and so the errors were expected to be mainly in the zonal direction. This result could indicate that processes other than the vertical mixing of momentum are not well represented in the model, such as the meridional transport of momentum.

In summary, within the equatorial waveband in the Pacific, the assimilations using the pressure correction method fit the thermal observations better near 50 m depth, have smaller time mean vertical velocities near 200 m depth, require smaller time mean assimilation increments at these depths and have a better equatorial undercurrent than the standard assimilation scheme. The gradients of the pressure correction field show that the assumption that most of the errors in the momentum equations come from incorrect wind stresses and their parameterisation in the vertical is not necessarily very accurate as there are might also be systematic errors in the horizontal transport of momentum.

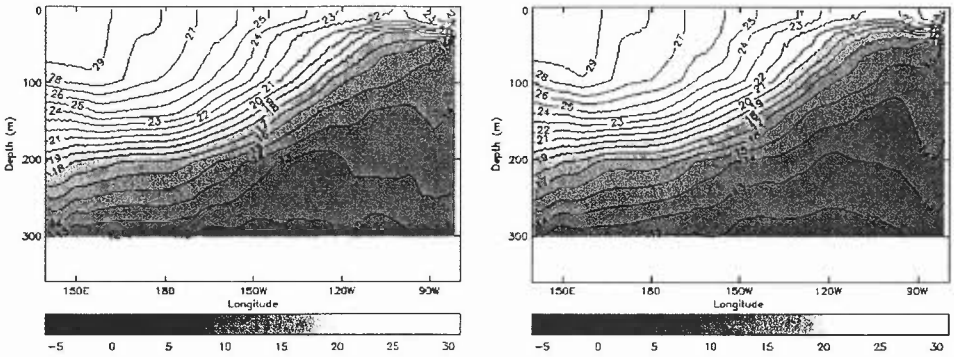

Figure B1. Annual mean (2nd Year) potential temperature (°C) cross-section along equator between 140°E – 90°W: (a) pressure correction, $\alpha = 0.1$ and (b) pressure correction, $\alpha = 0.3$.

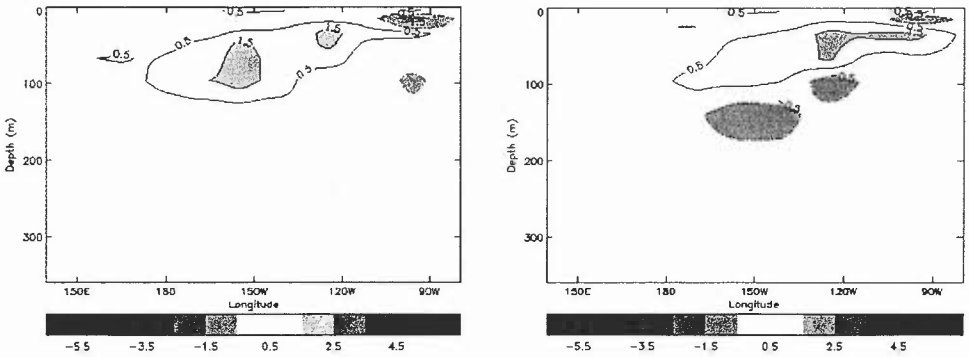

Figure B2. Annual mean (2nd Year) potential temperature increments (°C month^{-1}) cross-section along equator between 140°E-90°W: (a) pressure correction, $\alpha = 0.1$ and (b) pressure correction, $\alpha = 0.3$.

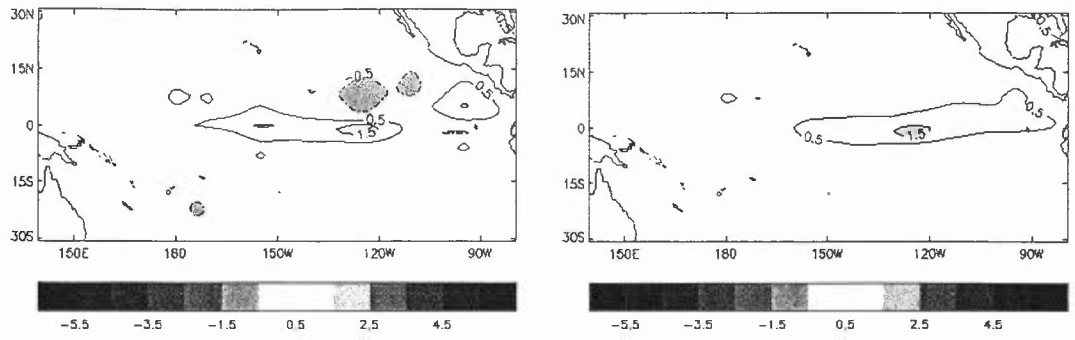

Figure B3. Annual mean (2nd Year) potential temperature increments (°C month^{-1}) field at about 50m: (a) pressure correction, $\alpha = 0.1$ and (b) pressure correction, $\alpha = 0.3$.

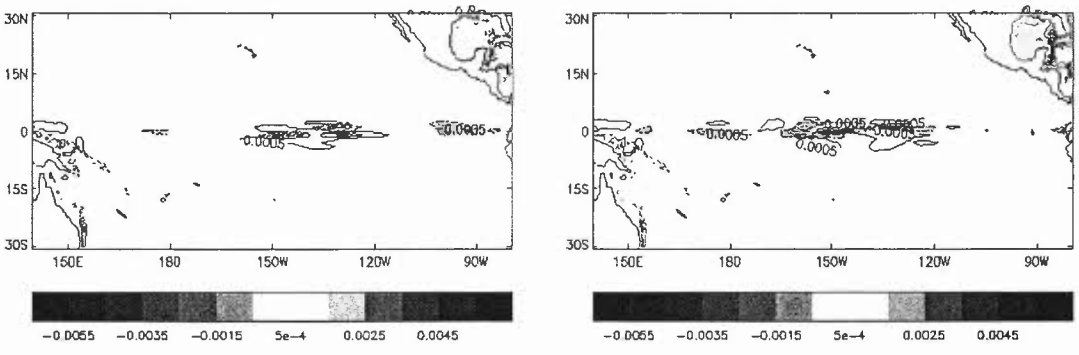

Figure B4. Annual mean (2nd Year) vertical velocities (cm s^{-1}) field at about 250m depth: (a) pressure correction, $\alpha = 0.1$ and (b) pressure correction, $\alpha = 0.3$.

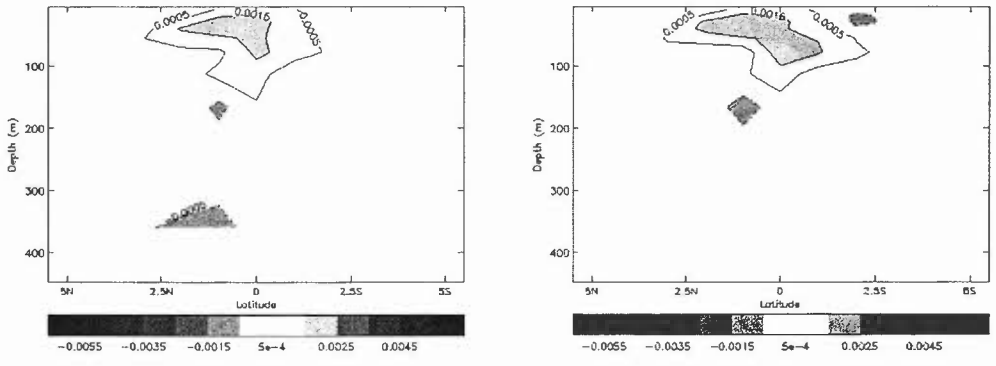

Figure B5. Annual mean (2nd Year) vertical velocities (cm s^{-1}) cross-section across equator at 110°W: (a) pressure correction, $\alpha = 0.1$ and (b) pressure correction, $\alpha = 0.3$.

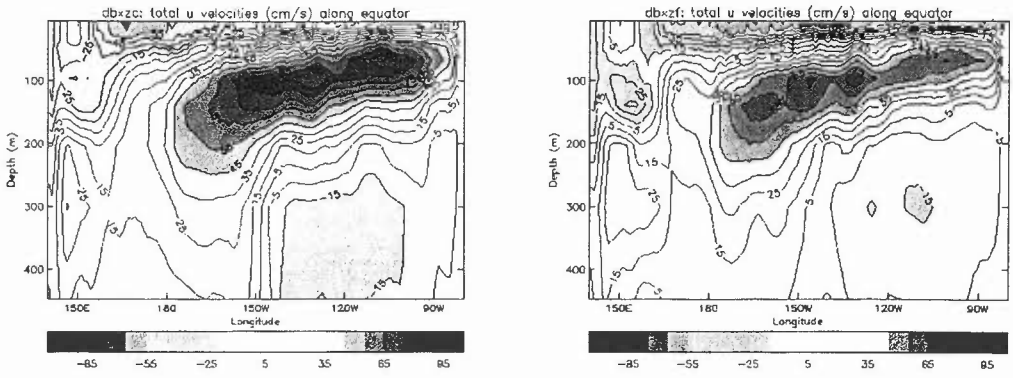

Figure B6. Annual mean (2nd Year) zonal velocity (cm s^{-1}) along the equator between 140°E-90°W: (a) pressure correction, $\alpha = 0.1$ and (b) pressure correction, $\alpha = 0.3$.

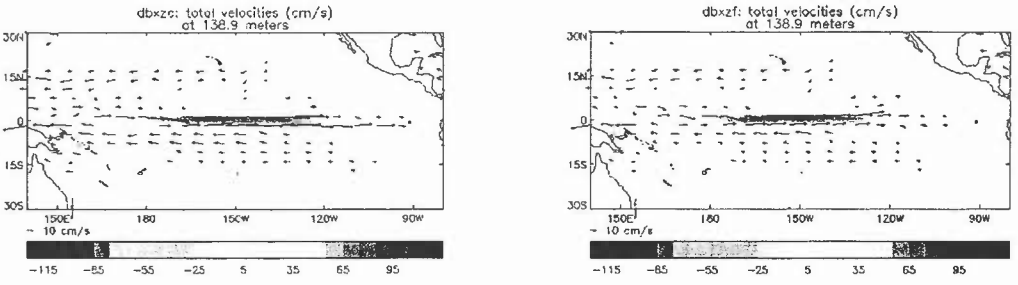

Figure B7. Annual mean (2nd Year) total velocity (cm s^{-1}) field at about 140m depth: (a) pressure correction, $\alpha = 0.1$ and (b) pressure correction, $\alpha = 0.3$.

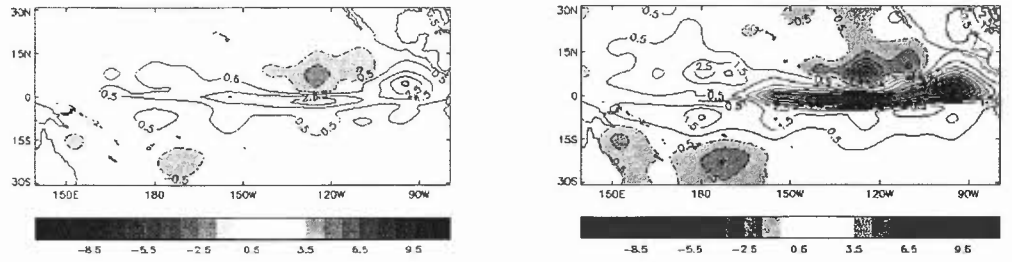

Figure B8. Annual mean (2nd Year) bias correction field (°C) at about 50m depth: (a) pressure correction, $\alpha = 0.1$ and (b) pressure correction, $\alpha = 0.3$.

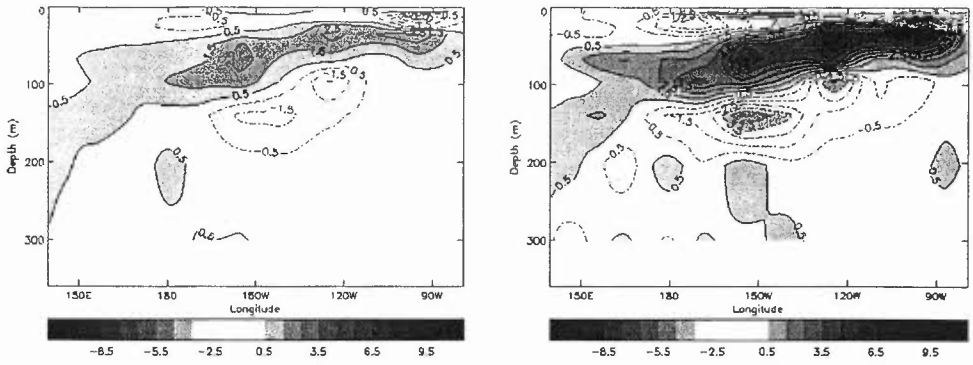

Figure B9. Annual mean (2nd Year) bias correction (°C) along the equator between 140°E-90°W: (a) pressure correction, $\alpha = 0.1$ and (b) pressure correction, $\alpha = 0.3$.

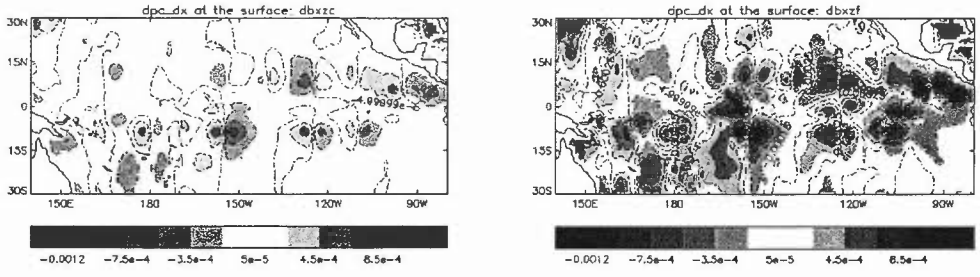

Figure B10. Annual mean (2nd Year) field of $\frac{dp^b}{dx}$: (a) pressure correction, $\alpha = 0.1$ and (b) pressure correction, $\alpha = 0.3$.

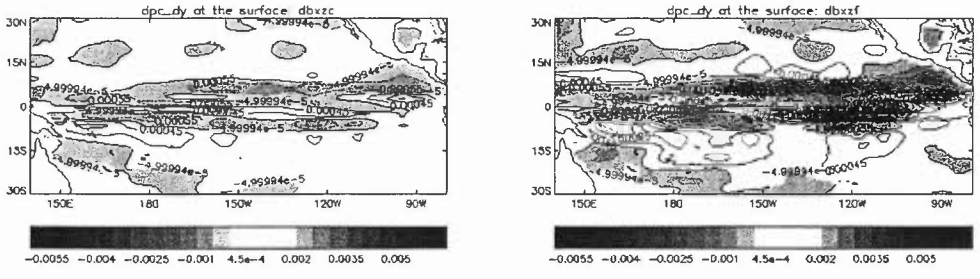

Figure B11. Annual mean (2nd Year) field of $\frac{dp^b}{dy}$: (a) pressure correction, $\alpha = 0.1$ and (b) pressure correction, $\alpha = 0.3$.

References

Bell, M.J., R.M. Forbes, and A. Hines, 2000. Assessment of the FOAM global data assimilation system for real-time operational ocean forecasting, *J. Mar. Syst.*, 24, 249-275.

Busalacchi, A.J., 1995. Oceanic observations, *Geophysical Magazine*, 1 (special issue), I-ii-1 - I-ii-16.

Cox, M.D., 1984. A primitive equation, 3-dimensional model of the ocean, *GFDL Ocean GroupTech. Rep. No. 1*, Geophysical Fluid Dynamics Laboratory, 143.

Daley, 1991. *Atmospheric Data Analysis*, Cambridge University Press.

Davis, H.C., and R.E. Turner, 1977. Updating prediction models by dynamical relaxation: an examination of the technique, *Quart. J. R. Met. Soc.*, 103, 225-245.

Dee, D.P., and A.M. Da Silva, (DDS) 1998. Data assimilation in the presence of forecast bias, *Quart. J. R. Met. Soc.*, 124, 269-295.

Derber, J.C., 1989. A variational continuous data assimilation technique, *Mon. Wea. Rev.*, 117, 2437-2446.

Février, S., C. Frankignoul, J. Sirven, M. Davey, P. Delecluse, S. Ineson, J. Macias, N. Sennéchael, and D.B. Stephenson, 2000. A multivariate intercomparison between three oceanic GCMs using observed current and thermocline depth anomalies in the tropical Pacific during 1982-1992, *J. Mar. Syst.*, 24, 249-275.

Friedland, B., 1969. Treatment of bias in recursive filtering, *IEEE Trans. Auto. Contr.*, AC-14, 359-367.

Gill, A.E., 1980. Some simple solutions for heat-induced tropical circulation, *Quart. J. R. Met. Soc.*, 106, 447-462.

Gill, A.E., 1982. *Atmospheric-Ocean Dynamics*, Academic Press.

Hellerman, S., and M. Rosenstein, 1983. Normal monthly wind stress over the world ocean with error estimates, *J. Phys. Oceanogr.*, 13, 1093-1104.

Ide, K., P. Courtier, M. Ghil and A.C. Lorenc, 1997. Unified notation for data assimilation: operational, sequential and variational, *J. Meteor. Soc. Japan.*

Ji, M., and A. Leetma, 1997. Impact of data assimilation on ocean initialisation and El Nino prediction. *Mon. Wea. Rev.*, 125, 742-753.

Levitus, S., R. Burgett, and T. Boyer, 1994. World ocean atlas 1994. Volume 3: Salinity and Volume 4: Temperature. *NOAH Atlas NESDIS 3 & 4.*

Lorenc, A.C., R.S. Bell, and B. MacPherson, 1991. The Met. Office analysis correction data assimilation scheme, *Quart. J. R. Met. Soc.*, 117, 59-89.

Pacanowski, R.C., and S.G.H. Philander, 1981. Parameterisationof vertical mixing in numerical models of tropical oceans, *J. Phys. Oceanogr.*, 11, 1443-1451.

Stockdale, T., D.L.T. Anderson, M. Davey, O. Delecluse, A. Kattenberg, Y. Kitamur, M. Latif, T. Yamagata, 1993. Intercomparison of tropical ocean GCMs, *WCRP*, 79.

Yu, L., and J.J. O'Brien, 1991. Variational assimilation of the wind stress drag coefficient and the eddy viscosity profile, *J. Phys. Oceanogr.*, 21, 709-719.